



## LJMU Research Online

Zhang, L and Rowe, WB

**Study of Convective Heat Transfer in Grinding Applied to Tool Carbide**

<http://researchonline.ljmu.ac.uk/id/eprint/12990/>

### Article

**Citation** (please note it is advisable to refer to the publisher's version if you intend to cite from this work)

**Zhang, L and Rowe, WB (2019) Study of Convective Heat Transfer in Grinding Applied to Tool Carbide. Journal of Manufacturing Science and Engineering, Transactions of the ASME, 142 (2). ISSN 1087-1357**

LJMU has developed **LJMU Research Online** for users to access the research output of the University more effectively. Copyright © and Moral Rights for the papers on this site are retained by the individual authors and/or other copyright owners. Users may download and/or print one copy of any article(s) in LJMU Research Online to facilitate their private study or for non-commercial research. You may not engage in further distribution of the material or use it for any profit-making activities or any commercial gain.

The version presented here may differ from the published version or from the version of the record. Please see the repository URL above for details on accessing the published version and note that access may require a subscription.

For more information please contact [researchonline@ljmu.ac.uk](mailto:researchonline@ljmu.ac.uk)

<http://researchonline.ljmu.ac.uk/>

# Study of convective heat transfer in grinding applied to tool carbide

Lei Zhang <sup>1\*</sup>, W. Brian Rowe <sup>2</sup>

*1 Key Laboratory of High Efficiency and Clean Mechanical Manufacture of Ministry of Education, National Demonstration Center for Experimental Mechanical Engineering Education, School of Mechanical Engineering, Shandong University, Jinan 250061, China*

*2 General Engineering Research Institute, Liverpool John Moores University, L3 3AF, UK*

*\* Corresponding author: School of Mechanical Engineering, Shandong University, Jinan 250061, China.*

*E-mail address: sirzhanglei@sdu.edu.cn.*

## Abstract

The grinding temperature is of great importance for quality and integrity of machined cemented carbide tool. Tool edge surfaces may be damaged by softening or being stressed, hardened, burned or cracked. Former research on grinding temperature prediction often made assumptions to simplify heat convection due to the grinding fluid. However, these simplifying assumptions can sometimes undermine the mathematical relationships between grinding conditions and surface temperature, particularly in low temperature grinding where fluid convection is most important. This paper is an attempt to provide an improved comprehensive thermal model for prediction of contact temperatures and for monitoring and control of thermal damage. Based on previous thermal model research, this paper tackles a key element of the thermal model for temperature prediction. It proposes a convective heat transfer model based on the classic theory of turbulent flow passing a plate. Theoretical predictions from the thermal model of turbulent flow developed in this paper are compared with experimental values. Predictions are further compared with values from a previously published laminar flow model. And it is shown that the new model leads to a significant reduction in predicted temperatures. The results suggest that the thermal model for turbulent flow provides a reasonable estimate of predicted temperature values within the region of the fluid boiling temperature. The estimates appear to be an improvement compared to the laminar flow thermal model. The turbulent flow thermal model is considered to improve estimates of background contact temperatures in grinding cemented carbide.

**Keywords:** Grinding; cemented carbides; thermal model; convection; turbulent flow

## 1. Introduction

Nowadays, 85% of all cemented carbide tools are coated [1]. Cemented carbide coated tools require high hardness, excellent wear resistance and long tool life. Cemented carbide, as an important material for coated tools, has a series of advantages such as high hardness, high abrasion resistance, high strength and good toughness. The cemented carbide and the coating must have a close union. Therefore, the surface processing quality of the cemented carbide substrate has an important influence on bonding strength of the substrate and the coating. Because of its high hardness, low thermal conductivity and linear expansion coefficient, brittleness and poor impact toughness, cemented carbide is difficult to machine. Machining is mainly by grinding [2]. In the grinding of cemented carbide, specific energy is very high.

Most of the energy is converted into heat in the grinding contact zone [3]. The temperature of the grinding zone increases rapidly [4]. When a critical temperature is exceeded, thermal damage such as burn and microcracks occur on the surface of the workpiece [5]. A rapidly increasing high temperature in grinding may have a serious influence on the surface of cemented carbide. The bonding quality of the coating applied with the cemented carbide substrate may be greatly affected. Therefore, it is important to study the grinding heat transfer and temperature in the grinding process in order to avoid grinding defects and to increase the bonding strength of the substrate and coating.

In the last several years, significant progress has been made in the quality of grinding cemented carbides. A resin bond diamond grinding wheel was used to grind cemented carbide material. In one study the grinding energy was proposed to divide into two parts: chip formation energy and plastic flow energy caused by ploughing [6]. Abdullah et al. studied creep feed grinding of cemented carbide with a resin bond diamond grinding wheel. The results showed that the surface roughness and wheel wear decrease with the increase of wheel speed. When the feed increased, the surface roughness was higher and wheel wear increased [7]. Sun and others studied the removal mechanism of nanostructured cemented carbide and its surface properties after grinding [8]. Ling Yin and others carried out plane grinding research on cemented carbide materials. The surface roughness, flatness and material removal rate of the workpiece after grinding were studied [9]. Denkena and others analyzed the effects of different grinding methods and different grinding wheels on the surface characteristics of cemented carbide cutting tools. The results showed that grinding has a strong influence on surface roughness, shape and residual stress of the sample [10]. In summary, there are only a few studies on grinding heat and grinding temperature for cemented carbide. The temperature of cemented carbide grinding is an important aspect of the cemented carbide grinding process and surface machining quality. The analysis of cemented carbide grinding temperature is of significance to the improvement of cemented carbide grinding technology.

In this paper, a mathematical model of the grinding heat flux and grinding temperature is established for cemented carbide grinding. Based on the theory of heat transfer, a convective heat transfer coefficient for turbulent flow in the grinding contact zone is derived. The grinding temperature was measured using an inserted artificial thermocouple. Thermal models for laminar coolant flow and for turbulent coolant flow for cemented carbide grinding under different grinding parameters are analyzed to predict the maximum temperature of the workpiece.

## **2. Grinding heat flux and temperature**

Thermal modelling has been extensively studied as a predictive tool to calculate grinding temperature in order to avoid heat damage [11-13]. The heat transfer is usually expressed in terms of heat flux because this enables convenient calculation of conduction and convection quantities. Basic definitions are briefly summarized below for clarity before developing the new turbulent convection model.

### **2.1 Grinding heat flux**

In a grinding process, the grinding power is almost all transformed into grinding heat. The total grinding heat flux is

$$q_t = \frac{F_t v_s}{bl_c} \quad (1)$$

Where  $F_t$ -tangential grinding force,  $v_s$ -wheel speed,  $b$ -grinding width,  $l_c$ -real grinding contact length.

Flux values are defined as rate of heat flow divided by the grinding contact area. The total grinding heat flux  $q_t$  generated in the contact zone is distributed to four heat sections: workpiece, wheel (abrasive), chips and fluid [13-15].

$$q_t = q_w + q_s + q_{ch} + q_f \quad (2)$$

Where  $q_w$ -grinding heat flux transferring into the workpiece,  $q_s$ -grinding heat flux transferring into the abrasive,  $q_{ch}$ -grinding heat flux transferring into the chips,  $q_f$ -grinding heat convection transferring into the grinding fluid,  $q_t$ -total grinding heat flux.

## 2.2 Grinding temperature

Some energy is immediately transported from the grinding zone by the chips and plays no further part in heat partition. From Equation (2),

$$q_t - q_{ch} = q_w + q_s + q_f \quad (3)$$

Fluid flux  $q_f$  initially enters the workpiece and then re-emerges from the workpiece in the convection cooling process, giving rise to a partition  $R_{ws}$  of heat flux between the work and grain.

$$R_{ws} = \frac{q_w + q_f}{q_w + q_s + q_f} \quad (4)$$

So that by equation (3) and (4),

$$R_{ws}(q_t - q_{ch}) = q_w + q_f = (h_w + h_f)(T_{max} - T_a) \quad (5)$$

Then

$$T_{max} = \frac{R_{ws}(q_t - q_{ch})}{h_w + h_f} + T_a \quad (6)$$

Where  $T_{max}$  is taken to be the maximum background temperature rise in the grinding contact zone,  $T_a$  is ambient temperature. The terms  $h_w$  and  $h_f$  are critical for heat conduction into the workpiece and into the fluid and are both are very important for low temperature grinding.

## 2.3 Work-grain heat partition

The work-grain partition ratio  $R_{ws}$  according to Rowe et al. 1997 [16] is expressed as,

$$R_{ws} = \left[ 1 + \frac{0.974 \cdot k_g}{\beta_w \cdot \sqrt{r_0 \cdot v_s}} \right]^{-1} \quad (7)$$

Where  $r_0$  - Effective contact radius of the abrasive grain,  $\beta_w = \sqrt{k_w \cdot \rho_w \cdot c_w}$  - Thermal property of workpiece,  $k_w$  - Thermal conductivity of the workpiece,  $\rho_w$  - Density of the workpiece,  $c_w$  - Specific heat capacity of the workpiece,  $k_g$  - Conductivity of the abrasive.

A conduction factor for the net heat flow into the workpiece  $h_w$  is defined as [22]

$$h_w = \frac{\beta_w}{C} \cdot \sqrt{\frac{v_w}{l_c}} \quad (8)$$

The factor  $C$  has a maximum value 1.13 for a uniform heat flux distribution or 1.06 for a triangular heat flux [17].

Heat flux to the chip is expressed as [22]

$$q_{ch} = \rho_w \cdot c_w \cdot T_{ch} \left( \frac{a_e \cdot v_w}{l_c} \right) \quad (9)$$

Where  $v_w$  - Feed speed,  $T_{ch}$  - Material chip temperature,  $a_e$  - Real cutting depth

#### 2.4 Contact length

The real contact length  $l_c$  for an elastic contact is given by [18],

$$l_c = \sqrt{8R_r^2 F_n' (K_s + K_w) d_s + a_e d_s} \quad (10)$$

Where  $F_n'$  - unit normal grinding force,  $d_s$  - wheel diameter,  $R_r$  - values of the roughness factor,  $K_s$  - elastic properties of wheel in the contact,  $K_s = \frac{1 - \nu_s^2}{\pi E_s}$ ,  $K_w$  - elastic

properties of material in the contact,  $K_w = \frac{1 - \nu_w^2}{\pi E_w}$ ,  $E_w, E_s$  - Young Modulus of material and wheel,  $\nu_w, \nu_s$  - Poisson ratio of material and wheel.

#### 2.5 Convective heat transfer coefficient for laminar flow

The convective heat transfer coefficient  $h_f$  of the laminar flow model (LFM) is derived as [19-20],

$$h_f \approx \frac{4}{9} \rho_f^{1/2} c_f^{1/3} \eta_f^{-1/6} k_f^{2/3} \sqrt{\frac{v_s}{l_c}} \quad (11)$$

Where  $\rho_f$  - fluid density,  $c_f$  - specific heat capacity of fluid,  $\eta_f$  - dynamic viscosity of fluid,  $k_f$  - thermal conductivity of fluid

### 3. Convective heat transfer coefficient for turbulent flow

#### 3.1 Turbulent flow development

Because the grinding depth and grinding arc length are usually small compared with the diameter and the curvature of the grinding wheel, the grinding arc length was assumed to be a straight line and the length of the line is  $l_c$ . The grinding fluid in the grinding arc is simplified to flow between two plates composed of the grinding wheel and the workpiece. For conventional operation, it is assumed that the grinding fluid in the grinding arc region is Newtonian with constant physical parameters. The convective heat transfer of the grinding fluid in the grinding arc zone is simplified to the convective heat transfer of the fluid flowing past the surface of the workpiece at a fixed speed. The grinding fluid is carried into the grinding arc zone by the grinding wheel, assuming that the flow velocity  $u_\infty$  of the grinding fluid is equal to the grinding wheel velocity  $v_s$ . As can be seen from Figure 1, when the fluid flows along the plate at a fixed speed  $v_s$ , the flow boundary layer thickness  $\delta$  is very thin at the beginning stage. Influenced by the viscous force of the grinding fluid, the fluid flows in an orderly stratified flow. The flow stage at this region is called the laminar flow region.

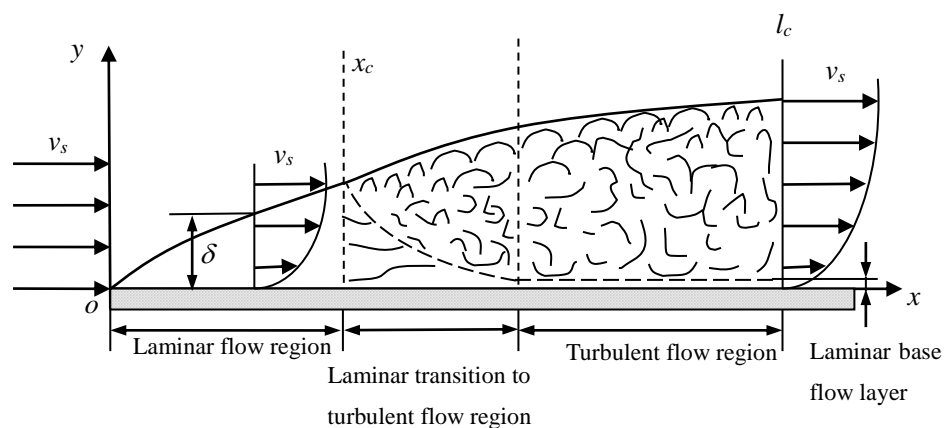


Figure 1 Schematic diagram of flow region development on the plate

With the increase of flow distance  $x$ , the influence of wall viscous force increases, the flow boundary layer thickness  $\delta$  increases and the inertia force becomes bigger than the viscous force, which makes the flow layer more and more unstable.

From position  $x_c$ , the fluid flow changes from laminar phase to turbulent, known as the transition region. Subsequently, the fluid flows in the X direction with an irregular pulsation, known as the turbulent flow region.

The position  $x_c$  is called the critical distance and can be calculated by the critical Reynolds number  $Re_c$ . The critical Reynolds number is generally between  $2 \times 10^5$  to  $3 \times 10^6$ . The laminar flow layer quickly transforms into a turbulent flow layer when the incoming flow disturbance is strong, the wall is rough or there is onset of fluid boiling. All three factors may apply in grinding. In particular, the wheel grits protruding through the pore space implies a very rough grinding wheel surface. This tends to reduce the critical Reynolds Number and increases the importance of introducing a turbulent model.[26]

$$Re_c = \frac{\rho_f u_\infty x_c}{\eta_f} \quad (12)$$

Where  $\rho_f$  is fluid density,  $\eta_f$  is fluid viscosity,  $x_c$  is critical distance;  $u_\infty$  is the fluid flow velocity.

### 3.2 Derivation of the convective heat transfer coefficient.

The convective heat transfer coefficient of grinding fluid for laminar flow past the workpiece surface at velocity  $u_\infty = v_s$  can be solved by using the momentum integral equation (13) and the energy integral equation (14). [26]

$$\frac{d}{dx} \int_0^\delta (u_\infty - u) u dy = \eta_f \left. \frac{\partial u}{\partial y} \right|_{y=0} \quad (13)$$

$$\frac{d}{dx} \int_0^{\delta_t} (t_\infty - t) u dy = a \left. \frac{\partial t}{\partial y} \right|_{y=0} \quad (14)$$

The turbulent flow analysis for the turbulent flow model (TFM) follows similar lines to the LFM analysis. However, the momentum and energy equations for turbulent flow are equations (15) and (16), [26]

$$u \frac{\partial u}{\partial x} + \eta \frac{\partial u}{\partial y} = (\eta + \varepsilon_m) \frac{\partial^2 u}{\partial y^2} \quad (15)$$

$$u \frac{\partial T}{\partial x} + \eta \frac{\partial T}{\partial y} = (a + \varepsilon_T) \frac{\partial^2 T}{\partial y^2} \quad (16)$$

where  $\varepsilon_m$  is the momentum diffusion rate of turbulent flow and  $\varepsilon_T$  is the thermal diffusion rate of turbulent flow.

Introduction of dimensionless values  $x^* = \frac{x}{l_c}$ ,  $y^* = \frac{y}{l_c}$ ,  $u^* = \frac{u}{u_\infty}$ ,  $v^* = \frac{\eta}{u_\infty}$ ,

$\Theta = \frac{T - T_w}{T_\infty - T_w}$  into equations (15) and (16),

$$u^* \frac{\partial u^*}{\partial x^*} + \eta \frac{\partial v^*}{\partial y^*} = \frac{1}{u_\infty l_c} (\eta + \varepsilon_m) \frac{\partial^2 u^*}{\partial y^{*2}} \quad (17)$$

$$u^* \frac{\partial \Theta}{\partial x^*} + \eta \frac{\partial \Theta}{\partial y^*} = \frac{1}{u_\infty l_c} (a + \varepsilon_T) \frac{\partial^2 \Theta}{\partial y^{*2}} \quad (18)$$

Then

$$\left. \frac{\partial u^*}{\partial y^*} \right|_{y^*=0} = \left. \frac{\partial \Theta}{\partial y^*} \right|_{y^*=0} \quad (19)$$

$$\left. \frac{\partial u^*}{\partial y^*} \right|_{y^*=0} = \left. \frac{\partial u}{\partial y} \right|_{y=0} \frac{l_c}{u_\infty} = \eta \left. \frac{\partial u}{\partial y} \right|_{y=0} \cdot \frac{l_c}{\eta u_\infty} = C_f \frac{Re_x}{2} \quad (20)$$

$$\left. \frac{\partial \Theta}{\partial y^*} \right|_{y^*=0} = - \frac{k_f}{(T_w - T_\infty)} \left. \frac{\partial T}{\partial y} \right|_{y=0} \frac{l}{k_f} = \frac{h_x l_c}{k_f} = Nu_x \quad (21)$$

Derived from equations (19), (20) and (21),

$$Nu_x = \frac{C_f}{2} Re_x \quad (22)$$

Where  $C_f$  is the resistance coefficient for turbulent flow over the plate [26],

$$C_f = 0.0592 Re_x^{-\frac{1}{5}} \quad (23)$$

Then derived from equations (22) and (23)

$$Nu_x = 0.0296 Re_x^{\frac{4}{5}} \quad (24)$$

The convective heat transfer in turbulent flow past a flat surface can be modeled as [26]

$$h_x = 0.0296 \frac{k_f}{x} Re_x^{\frac{4}{5}} Pr^{\frac{1}{3}} \quad (25)$$

If the surface temperature of the workpiece is higher than the critical onset temperature of fluid boiling but below the temperature at which the fluid burns out in the grinding contact zone, it is safe to assume that the entire fluid layer is in a turbulent state. Then the convective heat transfer coefficient of the TFM

$$h_f = \frac{1}{l_c} \int_0^{l_c} h_x dx \quad (26)$$

The wall temperature distribution in grinding arc zone is not constant. An approximate expression for average temperature rise is 2/3 maximum temperature. Thus, the average temperature rise must replace maximum temperature rise, thereby introducing a further factor of 2/3 into equation (26). Then the convective heat transfer coefficient for turbulent flow is

$$\bar{h}_f = 0.0247 \frac{k_f}{l_c} Re_{l_c}^{\frac{4}{5}} Pr^{\frac{1}{3}} \approx \frac{1}{40} \frac{k_f}{l_c} Re_{l_c}^{\frac{4}{5}} Pr^{\frac{1}{3}} \quad (27)$$

$Re_{l_c}$  is the Reynolds number of the fluid flowing along the grinding arc length.

$$Re_{l_c} = \frac{\rho_f v_s l_c}{\eta_f} \quad (28)$$

$Pr$  is the Prandtl number of the fluid.

$$Pr = \frac{c_f \eta_f}{k_f} \quad (29)$$

Where  $\rho_f$  is the fluid density,  $\eta_f$  is the fluid viscosity,  $k_f$  is the heat transfer coefficient of the fluid,  $v_s$  is the wheel velocity.

So, the convective heat transfer coefficient of TFM can be derived from equation (27), (28) and (29),

$$\bar{h}_f \approx \frac{1}{40} \rho_f^{4/5} c_f^{1/3} \eta_f^{-7/15} k_f^{2/3} \frac{v_s^{4/5}}{l_c^{1/5}} \quad (30)$$

### 3.3 Thermal model for turbulent flow

So that by equation (1), (6), (7), (8), (9) and (30), the maximum workpiece temperature for turbulent flow is

$$T_{\max} = \frac{F_t v_s - \rho_w \cdot c_w \cdot T_{ch} \cdot a_e \cdot v_w \cdot b}{\left(1 + \frac{0.974 \cdot k_g}{\sqrt{k_w \cdot \rho_w \cdot c_w \cdot r_0 \cdot v_s}}\right) \left(\frac{\sqrt{k_w \cdot \rho_w \cdot c_w \cdot v_w \cdot l_c}}{C} + \frac{1}{40} \rho_f^{4/5} \cdot c_f^{1/3} \cdot \eta_f^{-7/15} \cdot k_f^{2/3} \cdot v_s^{4/5} \cdot l_c^{4/5}\right) b} + T_a \quad (31)$$

The difference between the TFM and the LFM models derives from four variables, fluid density  $\rho_f$ , fluid viscosity  $\eta_f$ , wheel speed  $v_s$  and contact length  $l_c$ . In these experiments, wheel speeds were 10, 20 and 30 m/s. Wheel speed would provide another variable to test the model more extensively in the future.

## 4. Experimental procedure

The grinding experiments were carried out on a CNC grinding machine MKL7120, as shown in Fig. 2.

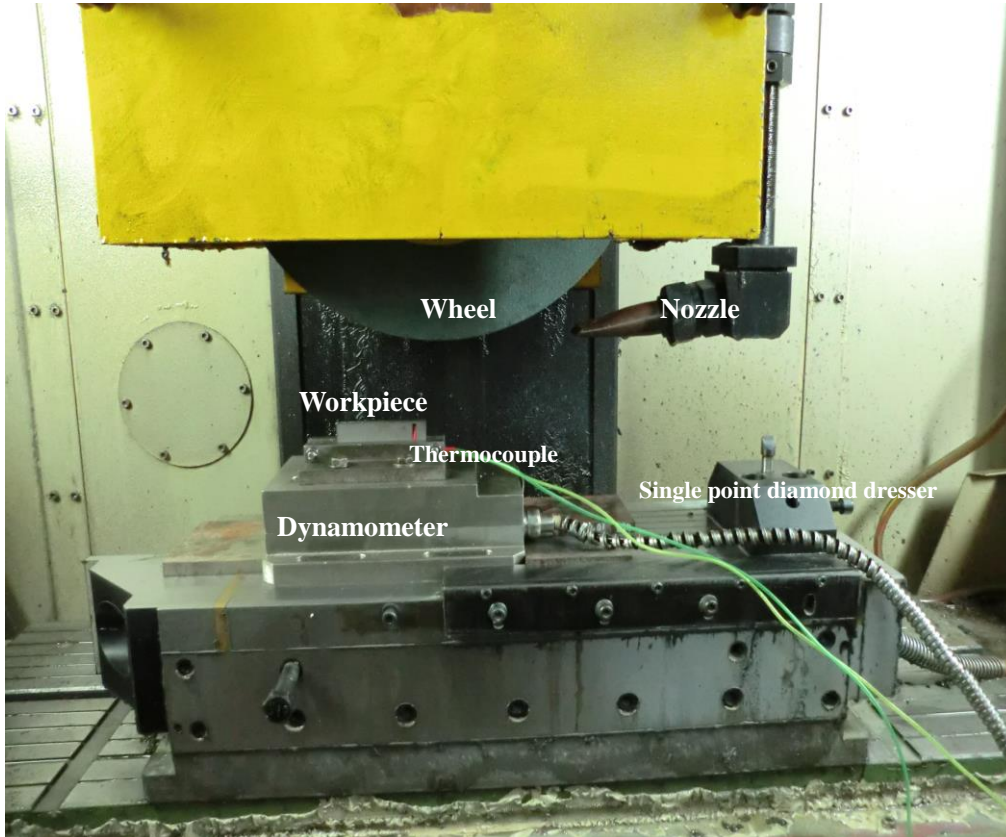


Figure 2 Grinding bench for force and temperature measurement

The grinding bench width×length was 200 mm×630 mm. The grinding table longitudinal travel was 650 mm, longitudinal feed speed was 10-20000 mm/min, and

minimum set unit was 0.001 mm. Vertical axis transverse stroke was 220 mm, feed speed was 0-2000 mm/min, and minimum set unit was 0.001 mm. Grinding head vertical feed speed was 0-1000 mm/min, the distance of the spindle center to table surface was 110-530 mm. Grinding head motor power was 9 kW, and maximum grinding speed was 3000 r/min. The coolant supply pump pressure was 8 bar, and maximum coolant flow was 80 L/min. The height of the nozzle was adjustable, and a regulating valve was used to control the coolant flow. In this experiment, a three-way piezoelectric quartz crystal dynamometer was used to measure the grinding force. The charge signals of the dynamometer were transformed into voltage signals by a charge amplifier (JY5003) and then collected by a NI data acquisition card (PCI-6024E). In order to measure the grinding force, the workpiece was mounted on a jig, the jig was fixed on the dynamometer, and the dynamometer was fixed on the working table of the grinder.

In experiments, a green silicon carbide grinding wheel GC80K5V was used to grind cemented carbide. The grinding wheel diameter was 355 mm, wheel width was 38.1 mm and bore diameter was 127 mm. A single grain diamond dressing pen was used for dressing. For dressing, the feed speed was 100 mm/min, the grinding wheel speed was 20 m/s, and the dressing depth was 20  $\mu\text{m}$  per dress. The grinding material was cemented carbide YG6. Cobalt content accounted for 6%, and WC and other minimum alloy components (TaC, Ni, etc.) accounted for 94%. The hardness was 90-91.5 HRA and the bending strength was 2800-3000 MPa. Water based emulsion was used in the grinding process. Physical and mechanical properties of cemented carbide and the coolant are shown in Table 1. The experimental scheme is shown in Table 2. Twenty-eight measurements were made, each of the seven shown were an average of 4 measurements.

Table 1 Physical and mechanical properties

| Parameters   | Cemented carbide | Silicon carbide wheel | Emulsion |
|--|------------------|-----------------------|----------|
| Thermal conductivity $k$ (W/mK)                                | 79.6             | 110                   | 0.56     |
| Density $\rho$ (kg/m <sup>3</sup> )                            | 14800            | 3210                  | 1000     |
| Specific heat capacity $c$ (J/kgK)                             | 209              | 1088                  | 4200     |
| Thermal diffusivity $\alpha$ (m <sup>2</sup> /s)               | 2.58e-5          | 3.15e-5               | 1.3e-5   |
| Thermal property $\beta$ (J/m <sup>2</sup> Ks <sup>0.5</sup> ) | 15691            | 19600                 | 1534     |
| Poisson ratio $\nu$  | 0.21             | 0.14                  | N/A      |
| Modulus of elasticity $E$ (N/m <sup>2</sup> )                  | 635e9            | 450e9                 | N/A      |
| Viscosity $\eta$ (Ns/m <sup>2</sup> )                          | N/A              | N/A                   | 0.001    |

Table 2 Grinding scheme

| No. | Table speed $v_w$<br>(mm/min) | Grinding depth $a_e$<br>( $\mu\text{m}$ ) | Wheel velocity $v_s$<br>(m/s) |
|-----|-------------------------------|---|-------------------------------|
| 1   | 100                           | 10  | 30                            |
| 2   | 100                           | 20  | 30                            |
| 3   | 100                           | 30  | 30                            |
| 4   | 200                           | 10  | 30                            |
| 5   | 300                           | 10  | 30                            |
| 6   | 200                           | 10  | 20                            |
| 7   | 200                           | 10  | 10                            |

Table 3 summarizes typical compositions of water-based fluids as loosely classified by Howes (1990) [21]. In this classification, emulsifiable oils often known as soluble oils contain 50-80% of mineral oil in the concentrate. The term ‘soluble’ is slightly misleading since a substantial proportion of emulsifier is required to achieve miscibility. True solutions do not require emulsifiers. Water-based fluids containing either synthetic or mineral oil are widely known as emulsions. Emulsions offer better cooling than neat oils but need frequent changing where low surface roughness must be maintained. The average temperature at which boiling commences in an oil/water emulsion is approximately 130°C [21]. A greater proportion of oil in the grinding fluid increases the burn-out temperature. In previous measurements by the author, maximum temperatures up to 180°C were recorded using emulsions before it became obvious that complete burn-out had occurred. [22] In the following experiments conducted on tool carbide, it was found that higher temperatures were achieved before complete burn-out occurred. It was assumed that the reason for the higher burn-out temperatures was the use of a much higher oil content in the emulsion. The corresponding temperature predictions were made assuming fluid convection was maintained throughout.

Table 3 Typical Compositions of Water-Based Fluids [22]

| Fluid                | % Composition of Concentrate |                             |             |                    |                         | Dilution<br>with Water |
|----------------------|------------------------------|-----------------------------|-------------|--------------------|-------------------------|------------------------|
|                      | Mineral<br>Oil               | EP/Lubrication<br>Additives | Emulsifiers | Coupling<br>Agents | Corrosion<br>Inhibitors |                        |
| Emulsifiable<br>oils | 50-80                        | 0-10                        | 10-40       | 0.5-3              | 0-10                    | 1:40-1:80              |
| Semi-<br>synthetics  | 5-30                         | 0-10                        | Up to 50    | 0.5-3              | 0-10                    | 1:50-1:80              |
| Synthetics           | Up to 5                      | -                           | 0-40        | 0.5-3              | Up to<br>40-1:200       | 1:10                   |

Grinding temperature was measured by the top wire method. The blind hole in the workpiece was pre-machined by ultrasonic processing. The distance between the blind hole end and the surface was  $51\mu\text{m}$ . The thermocouple was encased with a ceramic tube. The blind hole was fixed with a solidified adhesive to ensure that the thermocouple end was in contact with the workpiece, as shown in Fig. 3. In experiments, for example No.1, the cemented carbide was first ground two times and each grinding depth was  $20\mu\text{m}$ . Then the cemented carbide was ground at No.1 parameters in order to measure the temperature on the surface of the workpiece at grinding depth  $10\mu\text{m}$ . The same method was used for Nos.2-7.

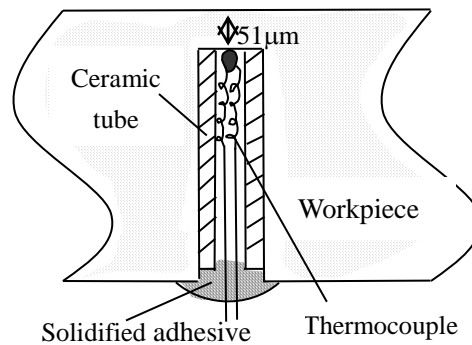


Figure 3 Schematic diagram of fixing the artificial thermocouple

The fixed temperature point method was used to calibrate the thermocouple. The thermocouple was placed in the incubator PHG-9146A. The temperature interval of the incubator was set to  $10^{\circ}\text{C}$ , and the corresponding voltage values of temperature increase were obtained respectively. The data were fitted and processed to obtain the thermoelectric potential-temperature calibration results. The thermocouple signals were amplified with a NI thermocouple amplifier module SCXI-1102. The thermoelectric potential data were collected by a NI data acquisition card PCI-6024E, and the grinding temperature was obtained by matching the thermocouple calibration results. The schematic of the experimental equipment is shown as Fig. 4.

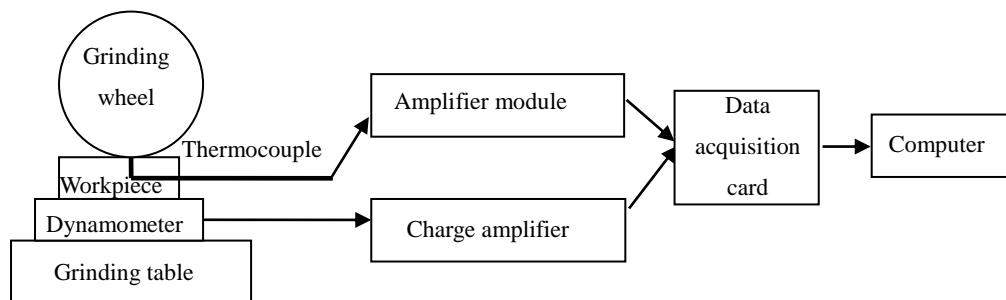


Figure 4 Schematic of experimental equipment

## 5. Results and discussion

The grinding force in both horizontal and vertical directions were measured by dynamometer. Since the grinding contact area is curved, the force measured needs to be transformed into tangential grinding force and normal grinding force. The conversion formula is as follows,

$$\begin{cases} F_n = \sin \theta F_y + \cos \theta F_z \\ F_t = \sin \theta F_z + \cos \theta F_y \end{cases} \quad (32)$$

$$\theta = \frac{2}{3} \arccos\left(1 - \frac{2a_e}{d_s}\right) \quad (33)$$

Where  $F_y$  is the horizontal force by the dynamometer,  $F_z$  is the vertical force by the dynamometer,  $F_n$  is the normal grinding force,  $F_t$  is the tangential grinding force,  $\theta$  stands for the angle between the vertical direction of the table and the normal grinding force,  $a_e$  is the grinding depth,  $d_s$  is the diameter of the grinding wheel. Grinding force by the dynamometer and grinding temperature signals are shown in Fig. 5.

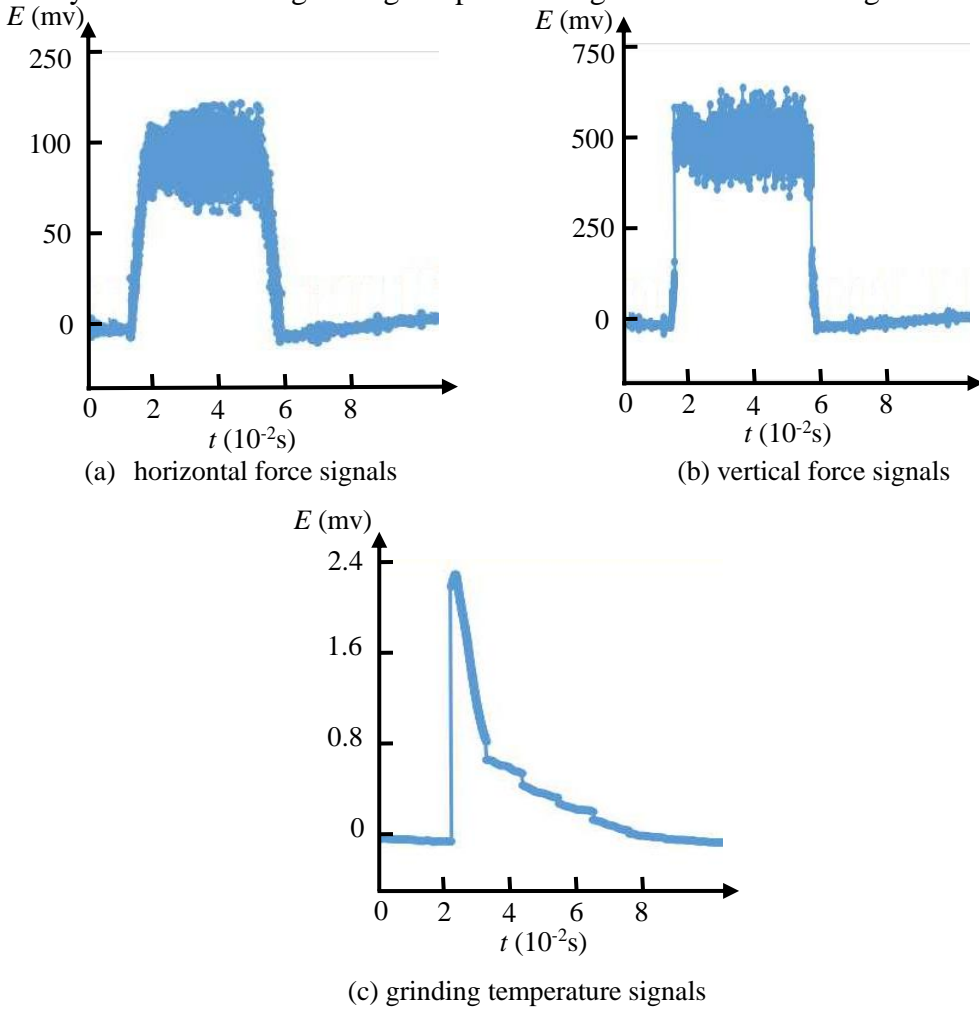


Figure 5 Grinding force and temperature electrical signals

Typical results of grinding force and temperature of cemented carbide YG6 by using green silicon carbide wheel are shown in Table 4. With an increase of wheel velocity, both the tangential grinding force and the normal grinding force decrease. With the increase of the wheel velocity, the cutting thickness of single abrasive grains decreases and the grinding force of single cutting edge is reduced, so the grinding force is reduced. The tangential grinding force and normal grinding force are increased with the increase of table speed. With the increase of the table speed, the cutting thickness of the abrasive grains increases, the grinding force of a single

abrasive cutting edge increases, and the number of effective abrasive grains increases in unit time, so the grinding force increases. With an increase in grinding depth, both the normal grinding force and the tangential grinding force are increased. With the increase of grinding depth, the cutting thickness of the abrasive grains increases, the grinding force of single abrasive grains increases, the contact arc length of grinding area is increased, so the grinding force increases.

Table 4 Experimental parameters and measurement results

| No.   | 1     | 2     | 3     | 4     | 5     | 6     | 7     |
|---|-------|-------|-------|-------|-------|-------|-------|
| Grinding wheel velocity $v_s$ (m/s)                       | 30    | 30    | 30    | 30    | 30    | 20    | 10    |
| Table speed $v_w$ (m/s)                                   | 0.1   | 0.1   | 0.1   | 0.2   | 0.3   | 0.2   | 0.2   |
| Grinding depth $a_e$ ( $\mu\text{m}$ )                    | 10    | 20    | 30    | 10    | 10    | 10    | 10    |
| Grinding width $b$ (mm)                                   | 6     | 6     | 6     | 6     | 6     | 6     | 6     |
| Tangential grinding force $F_t$ (N)                       | 14.3  | 26.3  | 33.4  | 37.9  | 47.4  | 54.5  | 76.4  |
| Normal grinding force $F_n$ (N)                           | 71    | 297.2 | 352.4 | 160.3 | 170.8 | 200.4 | 261   |
| Experimental temperature $T_{max}$ ( $^{\circ}\text{C}$ ) | 128.5 | 145.5 | 159   | 182   | 197.8 | 171.1 | 142.4 |

The critical distance  $x_c$  is an important value in considering using LFM or TFM analysis for workpiece temperature calculation. The critical Reynolds number of fluid flow between two plates is generally between  $2 \times 10^5$  to  $3 \times 10^6$  and wheel speeds were 10, 20 and 30 m/s. The range of the critical distance  $x_c$  calculated from Eqn. 12 is 6.7-300 mm. In these experiments, the range of grinding arc lengths is 3.04-6.23 mm. The reason is that the critical Reynolds number of grinding fluid in the grinding arc is different from that of flow between two plates because of a rough workpiece, rough grinding wheel, and entry conditions. The critical Reynolds number of the fluid in grinding is difficult to obtain for a specific range of values.

The comparison of experimental and theoretical temperatures from the LFM and TFM under different experimental schemes is shown in Table 5 and 6 respectively.

Table 5 Comparison of experimental and LFM theoretical temperatures

| No.   | 1     | 2     | 3     | 4      | 5      | 6     | 7     |
|---|-------|-------|-------|--------|--------|-------|-------|
| Grinding arc length $l_c$ (mm)                      | 3.04  | 5.56  | 6.23  | 4.05   | 4.15   | 4.42  | 4.94  |
| Total grinding heat flux $q_t$ (W/mm <sup>2</sup> ) | 23.6  | 23.65 | 26.81 | 46.79  | 57.11  | 41.10 | 25.78 |
| Heat flux to the chip $q_{ch}$ (W/mm <sup>2</sup> ) | 4.53  | 3.34  | 4.47  | 4.58   | 6.71   | 4.20  | 3.76  |
| Conduction factor for the net heat flow into        | 89994 | 66545 | 62865 | 110265 | 125858 | 99575 | 99839 |

|  |       |       |       |       |       |       |       |
|--|-------|-------|-------|-------|-------|-------|-------|
| the workpiece<br>$h_w$ (W/ (m <sup>2</sup> K)) |       |       |       |       |       |       |       |
| Work-grain partition<br>ratio $R_{ws}$         | 0.752 | 0.752 | 0.752 | 0.752 | 0.750 | 0.712 | 0.701 |
| LFM $h_f$ (W/(m <sup>2</sup> K))               | 47811 | 35438 | 33326 | 41305 | 40255 | 32241 | 21571 |
| Experimental surface<br>temperature $T$ (°C)   | 128.5 | 145.5 | 159   | 182   | 197.8 | 171.1 | 142.4 |
| LFM $T$ (°C)                                   | 124.1 | 169.7 | 194.6 | 229.4 | 247.5 | 219.3 | 147.1 |
| Error (%)                                      | 3.54  | 14.3  | 18.3  | 20.7  | 20.1  | 21.9  | 3.19  |

In the fourth, fifth and sixth groups of experiments, the error between the predicted and experimental values of grinding temperature is bigger than other groups. The main reason is that the surface grinding temperature is high in the fourth, fifth and sixth groups of experiments. In the grinding arc area, the grinding fluid at the boiling state seems to greatly increase the convection heat transfer coefficient. The convective heat transfer coefficient for LFM appears to be calculated inaccurately at the fluid boiling state.

The comparison of experimental and predicted results using the TFM is shown in Table. 6. The results show that the TFM provides reasonable temperature predictions at fluid boiling temperatures. Comparison with the predictions in Table 5 shows that predicted convection factors for the TFM are higher than for the LFM as would be expected given the reduced boundary layer thickness. The experimental and predicted temperature values of most groups were more consistent. The estimates using the TFM appear to be an improvement compared to the LFM thermal model at the fluid boiling temperature.

Table 6 Comparison of experimental and prediction results by thermal model of TFM

| No.   | 1     | 2     | 3     | 4      | 5      | 6     | 7     |
|---|-------|-------|-------|--------|--------|-------|-------|
| Grinding arc length $l_c$<br>(mm)   | 3.04  | 5.56  | 6.23  | 4.05   | 4.15   | 4.42  | 4.94  |
| Total grinding heat flux<br>$q_t$ (W/mm <sup>2</sup> )  | 23.6  | 23.65 | 26.81 | 46.79  | 57.11  | 41.10 | 25.78 |
| Heat flux to the chip $q_{ch}$<br>(W/mm <sup>2</sup> )  | 4.53  | 3.34  | 4.47  | 4.58   | 6.71   | 4.20  | 3.76  |
| A conduction factor for<br>the net heat flow into<br>the workpiece<br>$h_w$ (W/ (m <sup>2</sup> K)) | 89994 | 66545 | 62865 | 110265 | 125858 | 99575 | 99839 |
| Work-grain partition<br>ratio $R_{ws}$  | 0.752 | 0.752 | 0.752 | 0.752  | 0.750  | 0.712 | 0.701 |
| TFM coefficient $h_f$<br>(W/(m <sup>2</sup> K))   | 82353 | 73095 | 71284 | 77675  | 77305  | 55156 | 30985 |

|   |       |       |       |       |       |       |       |
|---|-------|-------|-------|-------|-------|-------|-------|
| Experimental surface temperature $T$ ( $^{\circ}\text{C}$ ) | 128.5 | 145.5 | 159   | 182   | 197.8 | 171.1 | 142.4 |
| TFM $T$ ( $^{\circ}\text{C}$ )                              | 103.2 | 129.4 | 145.2 | 188.9 | 206.1 | 189.8 | 138.0 |
| Error (%)   | 24.5  | 12.4  | 9.5   | 3.65  | 4.03  | 9.8   | 3.2   |

### 5.5 Measured fluid convection factors analysis

Convective heat transfer coefficients (CHTC) were measured inversely from Eq. (6) using measured temperatures. Table 7 lists the average experimental values of the CHTC from the tests. Because of measurement errors of grinding force, grinding power or temperature, the experimental CHTCs are estimated to be around  $\pm 5\%$  [23]. Figure 6 and 7 shows the CHTCs of LFM, TFM and inverse measurement within the measured temperature range of  $20^{\circ}\text{C}$ - $200^{\circ}\text{C}$ , with data from Table 5-7 and data from reference [19, 24, 25] respectively. The measured convection coefficients in Figure 6 tend to be larger than the predicted values for the LFM but lower than the values for the TFM. The predicted values are almost constant with increasing measured temperature. Examining Figure 6 in more detail, the measured values drop down for the two sets of data at the lowest temperatures entering the boiling zone but then increase as boiling temperatures increase. This is consistent with the known tendency for increase in convection factor with more vigorous bubbling and evaporation. However, as the surface temperature further increases, there comes a point where the fluid is rapidly boiled away; a condition known as fluid burn-out.

Table 7 Heat convective heat transfer coefficients  $h_f$

| No.  | 1                  | 2                  | 3                  | 4                  | 5                  | 6                  | 7                  |
|--|--------------------|--------------------|--------------------|--------------------|--------------------|--------------------|--------------------|
| Experimental surface temperature $T$ ( $^{\circ}\text{C}$ )                                  | 128.5              | 145.5              | 159                | 182                | 197.8              | 171.1              | 142.4              |
| Experimental convective heat transfer coefficient $h_f$ ( $\text{W}/(\text{m}^2 \text{K})$ ) | 46830<br>$\pm 5\%$ | 51786<br>$\pm 5\%$ | 55019<br>$\pm 5\%$ | 81404<br>$\pm 5\%$ | 75600<br>$\pm 5\%$ | 53175<br>$\pm 5\%$ | 22766<br>$\pm 5\%$ |

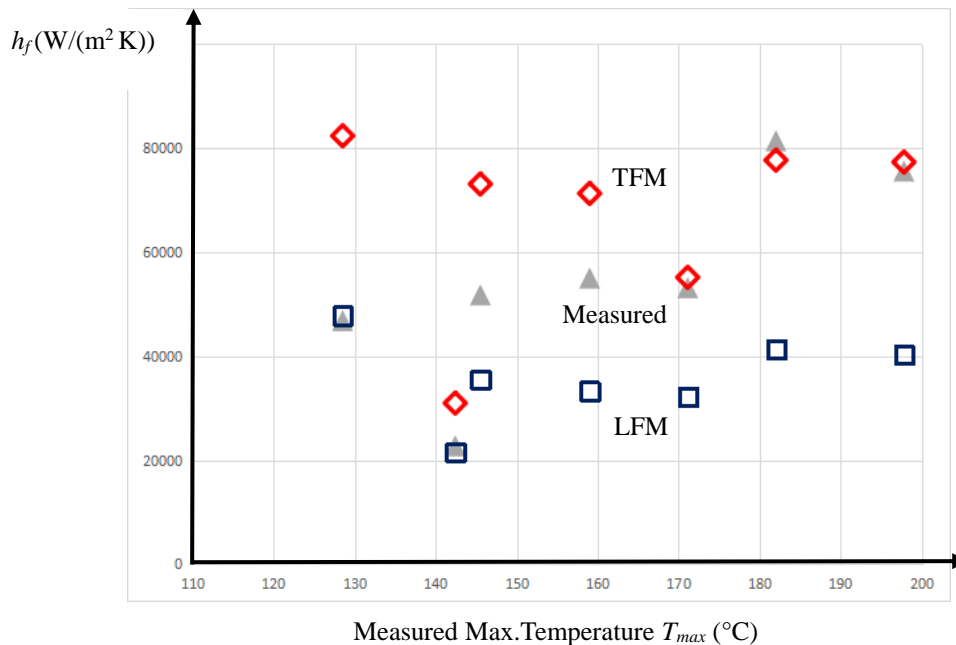


Figure 6 Fluid CHTCs of TFM, LFM and Measurement

The experimental values in Figure 7 show a wider temperature range including lower temperatures. The measured values for  $h_f$  reduce as temperatures approach  $100^{\circ}$ . The TFM predictions are clearly an improvement compared with the LFM predictions. The measured values of convection coefficients appear to reach a minimum at approximately  $120^{\circ}\text{C}$  before increasing up to approximately  $140^{\circ}\text{C}$ . At even higher temperatures the measured values reduce again towards zero as expected.

It appears probable that the difference between the results in Figure 6 and the results in Figure 7 is due to the much higher proportion of emulsified oil in the coolant used for the experiments in Figure 6. A larger proportion of oil in the coolant allows higher temperatures to be achieved before coolant burn-out occurs within the grinding contact. Previous results show that when burn-out occurs, the convection heat transfer coefficient is greatly reduced. This usually occurs above the top end of the temperature range for the results in Figure 6.

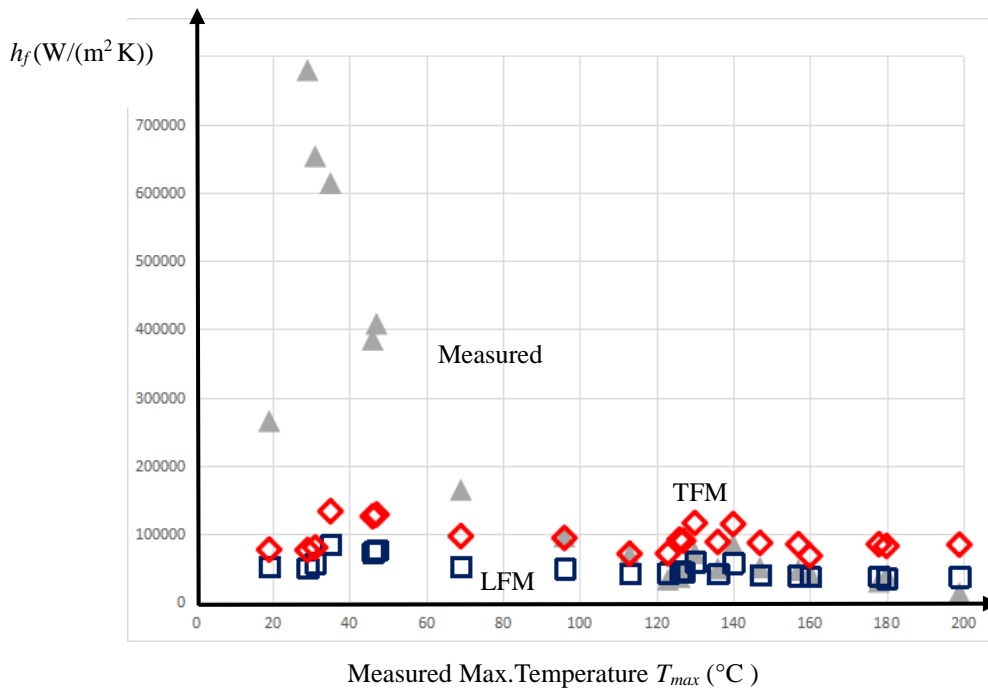


Figure 7 Fluid CHTCs of TFM, LFM and Measurement with water-based emulsion  
Data from Ref. [19, 24, 25].

The results presented in Figures 6 and 7 cover a wide range of carefully conducted experiments by several different researchers. Taken in their entirety, the results provide powerful evidence that high values of fluid convection factor are found in low temperature grinding and that a turbulent flow model is an improvement compared to a laminar flow model.

## 6. Conclusion

In this paper, a temperature prediction model of the grinding process has been developed with a convective heat transfer coefficient based on turbulent flow, the TFM. The proposed thermal model using the TFM results in a reduction in the grinding temperature prediction, as compared with that obtained by the LFM under the same conditions. Temperature predictions using the TFM at the fluid boiling stage are more consistent with experimental data than those of the LFM. It is confirmed that fluid convection substantially reduces grinding temperatures up to the point where fluid burn-out occurs. The grinding thermal models of TFM and LFM can be used to control the grinding quality by properly selecting the grinding parameters and fluid supply conditions. The development and refinement of fluid convection models are vital for the advancement of intelligent grinding technology and fluid supply equipment.

### **Acknowledgement**

This work was financially supported by National Natural Science Foundation of China (Grant No.51475276). Thanks are due to Mrs.Chunyu Wang for some experimental research work.

### **Reference**

1. Kirsten Bobzin. High-performance coatings for cutting tools. *CIRP Journal of Manufacturing Science and Technology*. 2017 (18): 1-9
2. J. Yang, J.J. Roa, M. Schwind, M. Odén, L. Llanes. Grinding-induced metallurgical alterations in the binder phase of WC-Co cemented carbides. *Materials Characterization*. 2017 Vol.134: 302-310
3. L. Zhang, P.Q. Ge, J.H. Zhang, Z.J. Zhu and Z.Y. Luan, Experimental and simulation studies on temperature field of 40Cr steel surface layer in grind-hardening, *International Journal of Abrasive Technology*, 2007, Vol. 1: 187-197
4. L. Zhang, P. Q. Ge, J. F. Meng, J. H. Cheng, M. Wang. New Heat Flux Model in Surface Grinding. *Materials Science Forum*. 2004, Vol.471-472: 298-301
5. Jianhua Zhang, Peiqi Ge, Tien-Chien Jen, Lei Zhang. Experimental and Numerical Studies of AISI1020 Steel in Grind-hardening. *International Journal of Heat and Mass Transfer*. 2009. Vol. 52 (3-4): 787-795
6. O. Zelwer, S. Malkin. Grinding of WC-Co Cemented Carbides. *Journal of Engineering for Industry*. 1980, Vol.102: 209-220
7. Amir Abdullah, Abbas Pak, Mahdi Farahi, et al. Profile Wear Of Resin-Bonded Nickel-Coated Diamond Wheel and Roughness in Creep Feed Grinding of Cemented Tungsten Carbide. *Journal of Materials Processing Technology*. 2007, Vol.183: 165-168
8. H. Q. Sun, R. Irwan, H. Huang, et al. Surface Characteristics and Removal Mechanism of Cemented Tungsten Carbides in Nanoscratching. *Wear*. 2010: 1-9
9. Ling Yin, A. C. Spowage, K. Ramesh, et al. Influence of Microstructure on Ultraprecision Grinding of Cemented Carbides. *International Journal of Machine Tools & Manufacture*. 2004, Vol. 44: 533-543
10. B. Denkena, C. Schmidt, M. Kruger. Experimental investigation and modeling of thermal and mechanical influences on shape deviations in machining structural parts. *International*

Journal of Machine Tools & Manufacture. 2010: 1015-1021

11. W. B. Rowe, M. N. Morgan, S. C. E. Black and B. Mills: A Simplified Approach to Thermal Damage in Grinding. *Annals of the CIRP*. 1996, Vol.45 (1): 299–302
12. T. Jin and D. J. Stephenson. A Study of the Convection Heat Transfer Coefficients of Grinding Fluids. *CIRP Annals -Manufacturing Technology*. 2008, Vol.57: 367-370
13. W. B. Rowe. Temperature Case Studies in Grinding Including an Inclined Heat Source Model. *Proceedings of I Mech E, Part B, J of Engineering Manufacture*. 2001, Vol.215: 473-491
14. M. N. Morgan, L. Barczak and A. Batako. Temperatures in fine grinding with minimum quantity lubrication (MQL). *Int J Adv Manuf Tech*. 2012, Vol.60: 951-958.
15. T. Jin, D. J. Stephenson and W. B. Rowe. Estimation of the Convection Heat Transfer Coefficient of Coolant within the Grinding Zone. *Proceedings of I Mech E, Part B, J of Engineering Manufacture*. 2003, Vol. 217: 397-407
16. W. B. Rowe, S. Black, B. Mills, M. N. Morgan and H. S. Qi. Grinding Temperatures and Energy Partitioning. *Proceedings of the Royal Society, Part A*. 1997, Vol.453: 1083-1104.
17. W. B. Rowe. Temperatures in Grinding-A Review. *Journal of Manufacturing Science and Engineering*. 2017, Vol. 139: 1-6
18. W. B. Rowe, H. S. Qi, M. N. Morgan and H.W. Zhang. The Effect of Deformation in the Contact Area in Grinding. *Annals of CIRP*. 1993, Vol.42 (1): 409–412.
19. Lei Zhang, W. B. Rowe, M. N. Morgan. An Improved Fluid Convection Solution in Conventional Grinding. *Proceedings of the Institution of Mechanical Engineers, Part B, J. of Engineering Manufacture*. 2013, Vol.227 (6): 832-838
20. Lei Zhang and M. N. Morgan. A Model of the Fluid Convective Cooling in Grinding Process. *Advanced Materials Research*. 2013, Vol. 797: 299-304
21. Howes, T. D. Assessment of the cooling and lubricative properties of grinding fluids. *Ann. CIRP*. 1990, Vol. 39 (1): 313-316.
22. Rowe, W. B. *Principles of Modern Grinding Technology*. Elsevier. Oxford, UK. 2014: 129.
23. Jin, T. and Stephenson, D. J. A Study of Convection Heat Transfer Coefficients of Grinding Fluids. *CIRP Ann. Manuf. Technol*. 2008, Vol.57 (1) :367-371.
24. B. Lin, M. N. Morgan, X. W. Chen and Y. K. Wang. Study on the Convection Heat Transfer Coefficient of Coolant and the Maximum Temperature in the Grinding Process. *Int. J. Adv. Man. Tech*. 2009, Vol. 42 (11) : 1175-1186.
25. L. Barczak, A. Batako and M. Morgan. A Study of Plane Grinding Under MQL. *Int. J. Mach. Tools Manuf*. 2010, Vol.50 (11) : 977-985.
26. Shiming Yang, Wenquan Tao. *Heat transfer*. Higher Education Press. Beijing, P.R.C. 2003.